RSC Advances

ROYAL SOCIETY OF CHEMISTRY

www.rsc.org/advances

RSC Advances

ARTICLE

N-type SnO_2 Nanosheets Stand on P-type Carbon Nanofibers: A Novel Hierarchical Nanostructures Based Hydrogen Sensor

Received 00th January 20xx,
Accepted 00th January 20xx

DOI: 10.1039/x0xx00000x

www.rsc.org/

Zhaojie Wang,[a] Siyuan Liu,[b] Tingting Jiang,[c] Xiuru Xu,[b] Jun Zhang,[d] Changhua An,[a,*] and Ce Wang,[b,*]

High-efficient chemical sensors based on various nanostructures have attracted considerable attention owing to their practical applications in industry and in daily lives of human beings. One of the most interesting and urgent challenges is to synthesize hierarchical heterostructured nanomaterials with high performance. In this paper, hierarchical p-n junction nanostructures made of n-type SnO_2 nanosheets standing on p-type carbon nanofibers have been successfully fabricated by combining electrospinning technique and hydrothermal method. The morphologies of the SnO_2 nanosheets can be easily controlled through tuning experimental conditions such as hydrothermal reaction time. The gas sensing performances based on the hierarchical nanostructures with hydrogen as target molecules have been evaluated. The expected sensing performances (e.g., low operating temperature, large response and fast response-recovery behaviors) have been achieved owing to the synergy effect between SnO_2 nanosheets, CNFs and the well-defined shaped hybrid nanostructures.

Introduction

Among many different gases, the rapid detection of dangerous gases such as hydrogen is technologically essential as these gases are typically colorless, odorless, and highly explosive in a wide range. In this regard, highly-efficient chemical sensors (CSs) have been extensively explored and developed, including solid electrolyte gas sensors, metal oxide gas sensors, electrochemical gas sensors and graphene-based gas sensors.[1-6] Even so, there are still some unresolved issues for these gas sensors such as the relatively high operating temperature (usually over 300°C for SnO_2-based gas sensors), the long response and recovery time. High operating temperature would impose a substantial safety risk during the gas detection and put a noteworthy restriction on practical utilization of these sensors due to their corresponding energy consumption, being inconsistent with the green energy concept. Also, fast response speed is necessary so that the users can receive an advance warning when the dangerous gas is detected.

Recent advent of nanotechnology provides a further impetus to the development of nanostructured materials as sensing elements (SEs). Primary working principal of these SEs is that their electrical conductance is changed by the interaction between the target molecules and chemisorbed oxygen species on the surface. Prompted by such important factor, construction of highly-efficient CSs with one-dimensional (1D) nanomaterials as SEs is of current interest owing to the fact that 1D nanostructures can exhibit not only better electrical transport over zero-dimensional nanomaterials but also improved interfacial areas between the target molecules and the chemisorbed oxygen species on the surface than two-dimensional nanostructures, leading to significant increase in the sensing signal, rapid response/recovery behavior, and good stability.

By assembling of different nanostructure on the core 1D nanomaterials, such as nanobelts, nanowires, nanofibers and so forth, hierarchical hybrid structures were produced.[7-9] Such heterostructures retain the merits of core material and provide additional properties specific to the decoration outside.[10-13] In the field of gas sensors application, heterostructured nanomaterials based on 1D backbones are promising because more mechanisms are likely to be involved during gas molecules interacting with them.[14] First, the depletion layers along the backbone and the surface structure can be modulated by the adsorption and desorption process of gas molecules. Second, modulation in resistance will mainly occur in the backbone due to the continuous structure. Third, the potential barriers between the homojunction overlapped in the network can also be modulated. Fourth, besides the homojuctions, the heterojunctions at the interface between the backbone and the surface structure will provide an additional potential barrier. All these four components are not completely independent, suggesting that the resistance change will be greater

[a] Department of Materials Physics and Chemistry, College of Science, China University of Petroleum, Qingdao, 266580, China.
[b] Alan G. MacDiarmid Institute, College of Chemistry, Jilin University, Changchun, 130012, China
[c] Department of Catalysis Science and Engineering, School of Chemical Engineering and Technology, Harbin Institute of Technology, Harbin 150001, China
[d] State Key Laboratory of Heavy Oil Processing, College of Chemical Engineering, China University of Petroleum, Qingdao, 266580, China
* Corresponding Author: anchh@upc.edu.cn (C. A.); cwang@jlu.edu.cn (C. W.)
† Electronic Supplementary Information (ESI) available: TEM images and EDS analysis of the prepared hierarchical p-n junction nanostructures, the morphology and sensing performances of SnO_2 microspheres assembled from SnO_2 nanosheets. See DOI: 10.1039/x0xx00000x

in heterostructured materials during the adsorption and desorption process of gas molecules, consequently improved sensing capabilities as expected.

Recently, 1D electrospun nanostructures based SEs have been widely explored in fabricating diverse CSs. For example, Li and co-workers constructed rapid and stable humidity sensors based on LiCl-doped TiO_2 electrospun nanofibers.[15] Wang et al. fabricated sensitive hydrogen sensors based on p-NiO/n-SnO_2 electrospun nanofibers.[16] Wang and his groups achieved high-performance ammonia sensors based on WO_3 electrospun nanofibers.[17] Although great strides have been achieved in the past several years, little attention has been paid to the exploration of gas sensing performances based on hierarchical p-n junction nanostructures, which possess the capacity to provide a more beneficial structure and thus introduce greater functions.[18-21]

In this study, we have demonstrated a novel CSs with hierarchical p-n junction nanostructures as SEs, in which n-type SnO_2 nanosheets were decorated on the surface of p-type carbon nanofibers by combining electrospinning and hydrothermal method. Gas sensing properties were investigated systematically with hydrogen as target molecules. Greatly improved gas sensing properties such as high response, low operable temperature, fast response/recovery behavior and good selectivity have been obtained. We believe that our method will offer a powerful platform to better understand the configuration/structure and their effect on sensing performances.

Experimental

Chemicals

Polyacrylonitrile (PAN, Mw=150,000), $SnCl_2 \bullet 2H_2O$ and mercaptoacetic acid were purchased from Aldrich Reagent Co.. N, N-dimethyl formamide (>95%) and HCl (36-38%) were purchased from Beijing Chemical Company (China). Urea was purchased from Tianjin Chemical Company (China). All chemicals were used as received without any further purification.

Preparation of SnO_2 nanosheets decorated CNFs

PAN nanofibers were electrospun from the solutions with 8% concentration at 15 kV with a power supply (gamma high-voltage supply, ES30-0.1P) and collected on a ground aluminium target 20 cm away from the orifice. The obtained fibers were degassed for at least 24 h to remove the residue solvent. The electrospun PAN nanofibers were then experienced a pre-oxidation procedurally and carbonization at 800℃ in a flow of argon gas finally.[22]

CNFs (6 mg) were added into 10 mM mercaptoacetic acid solution (40 mL), followed by the addition of $SnCl_2$ (100 mg), urea (0.5 g), and HCl solution (37 wt%, 0.5 mL). After stirring for 2 minutes, the reaction mixture was then transferred into a 60 mL Teflon-lined stainless steel autoclave and kept at 120℃ for different times. After the reaction was terminated, the autoclave was cooled to room temperature naturally. The obtained black precipitate was collected by centrifugation, washed thoroughly with ethanol, and dried at 60℃ overnight. The products were calcined at 300℃ in air for 2 h with a heating rate of 1℃/min in order to obtain a highly crystalline SnO_2 nanosheets.

Characterization

The fibrous mat was characterized by means of transmission electron micrographs (TEM, JEX-1200EX microscope.) and X-ray diffraction (XRD, Siemens D5005 diffractometer using Cu Ka radiation). Thermal gravimetric analysis (TGA) was employed to evaluate the weight loss of the samples in air under a heating rate of 5℃/min through thermal analyzer (Perkin-Elmer PYRIS 1).

Sensor devices preparation and measurement

The as-prepared hierarchical p-n junction nanostructures were mixed with deionized water in a weight ratio of 100:25 to form a paste. The paste was coated onto a ceramic tube on which a pair of gold electrodes was previously printed, and then a Ni-Cr heating wire was inserted in the tube to form a side-heated gas sensor. Gas sensing properties to H_2 were measured using a custom-made static test system. Saturated H_2 was injected into a glass test chamber (about 20 L in volume) by a syringe through a rubber plug. After fully mixed with air (relative humidity was about 25%), the sensor was put into the test chamber. When the sensitivity reached a constant value, the sensor was taken out to recover in air. Electrical properties of the sensors were measured using CGS-8 intelligent test system (Beijing Elite Tech Co. Ltd., China). Sensor response (S) was measured between 120 and 280℃ by comparing the resistance of the sensor in dry synthetic air (Ra) with that in target gases (Rg). The time taken by the sensor to achieve 90 % of the total resistance change was defined as response time in the case of adsorption or recovery time in the case of desorption.

Results and discussion

The morphology of samples obtained at different hydrothermal reaction time was characterized as shown in Fig.1. These typical SEM images show that all the products consist of 1D nanostructures

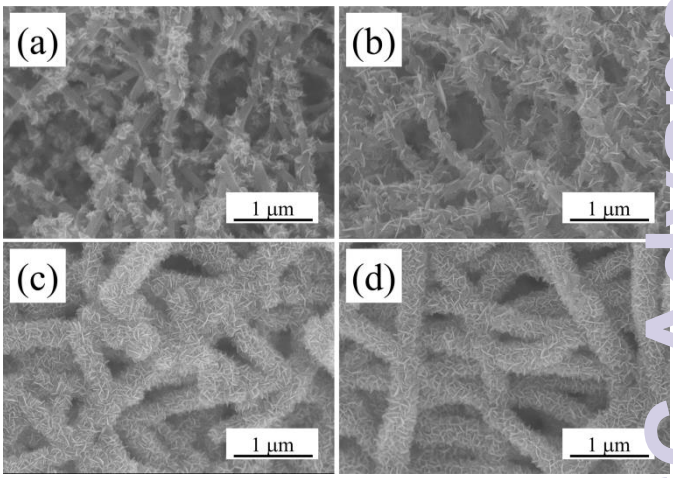

Fig. 1 SEM images of the hierarchical p-n junction nanostructures at different hydrothermal reaction times (a) 3h, (b) 6 h, (c) 12 h, (d) 24 h.

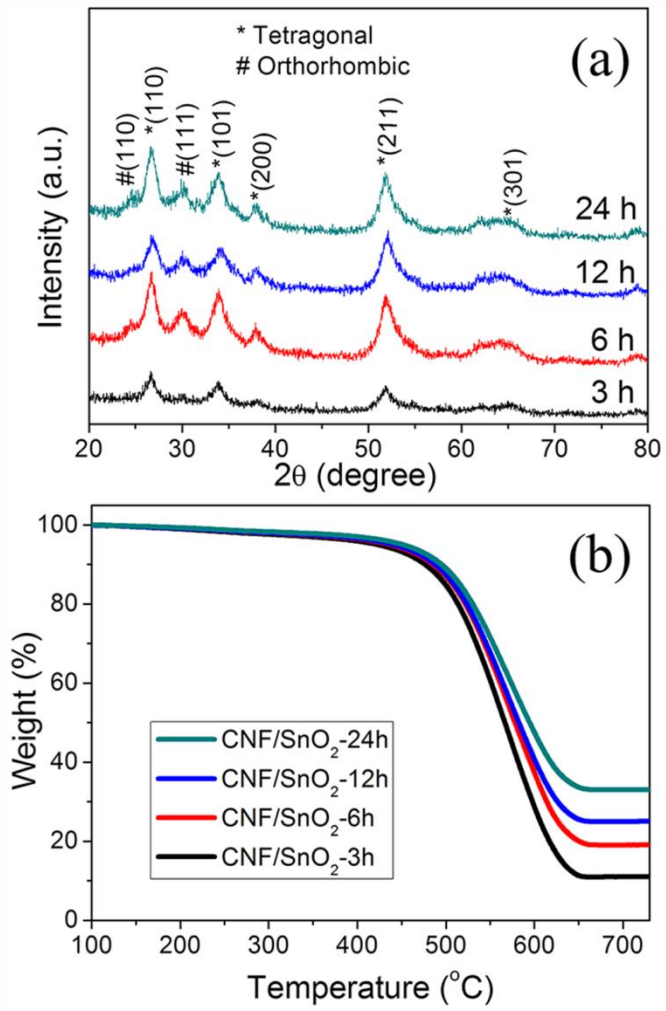

Fig. 2 (a) XRD and (b) TGA patterns of the obtained hierarchical p-n junction nanostructures at different hydrothermal reaction times.

with different diameters in a range of 150～500 nm and each 1D backbone is decorated by a large amount of nanosheet subunits. The heterostructures are formed uniformly throughout the longitudinal axis of the CNF. Further studies reveal that the hydrothermal reaction time can be used to control the size of the "hairy" structure easily (Fig. S1†). At the initial stage of the reaction, lots of burrs were grafted around the backbones of CNF (Fig. 1a). Prolonging the reaction time, it results in the evolution of the burrs into nanosheets with larger width and only several nanometers in thickness. It is worth noting that the boundary between CNFs backbone and the outer shell of the SnO_2 nanosheets is not discernible. In the current synthesis system, mercaptoacetic acid acts as a molecular linker that binds initially formed SnO_2 to the CNFs.[23] Due to the smaller lateral dimension of the SnO_2 nanosheets, they appear to stand upright on the carbonaceous backbone rigidly with an intense arrangement.

Fig. 2a shows the XRD patterns of the chemical compositions of the products obtained at different reaction times. Besides the rutile phase of SnO_2 (JCPDS no. 41-1445), characteristic diffraction peaks

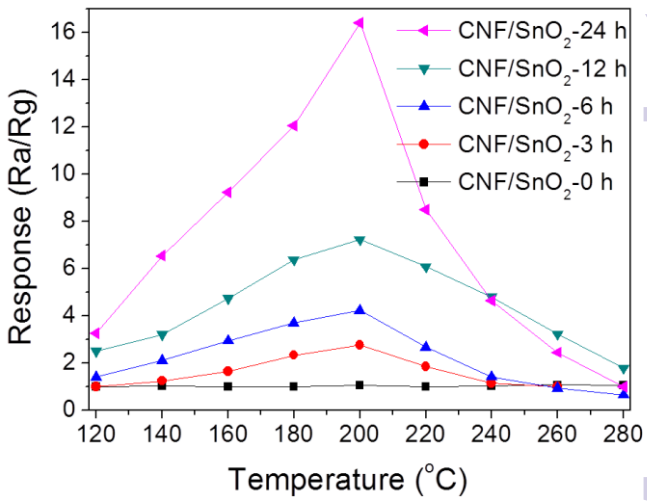

Fig. 3 Responses of the sensors based on the as-prepared hierarchical p-n junction nanostructures at different hydrothermal reaction times against 100 ppm H_2 as a function of operating temperatures.

of orthorhombic phase (JCPDS no. 29-1484) can also be distinguished.[24] The protuberance observed at 2θ =24.4° and the additional peak between rutile (110) and (101) can be assigned as orthorhombic (110) and (111) respectively. Low crystallinity results in the weak diffraction intensity and broadening in width of every diffraction peak. The broad peak after 2θ=60° can be attributed to the overlap of several closely diffraction peaks including tetragonal (310) and (301) planes, and orthorhombic (222), (023), (132) and (311) planes. The EDS analysis has been carried out as shown in Fig. S2. Fig. 2b gives the weight fractions of CNFs in the hybrid material. After reaching 700℃, it was found that the weight loss (wt%), resulted from the decomposition of carbon nanofibers, decreases

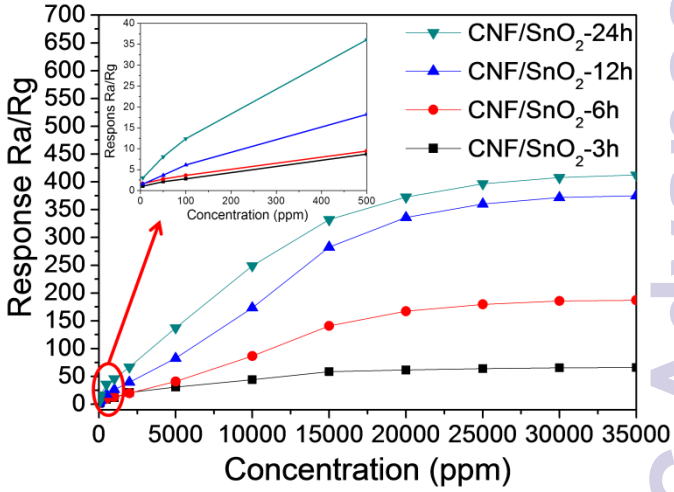

Fig. 4 Linear plots of the response of the sensors based on the hierarchical p-n junction nanostructures with different hydrothermal reaction time against H_2 in the range of 5 ppm – 3.5% at 200℃.

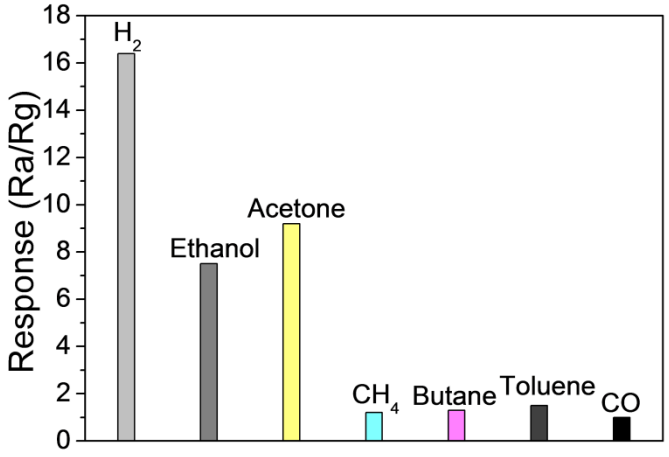

Fig. 5 Response of the optimized sensor to 100 ppm different gases (H_2, ethanol, acetone, CH_4, butane, toluene and CO) at 200℃.

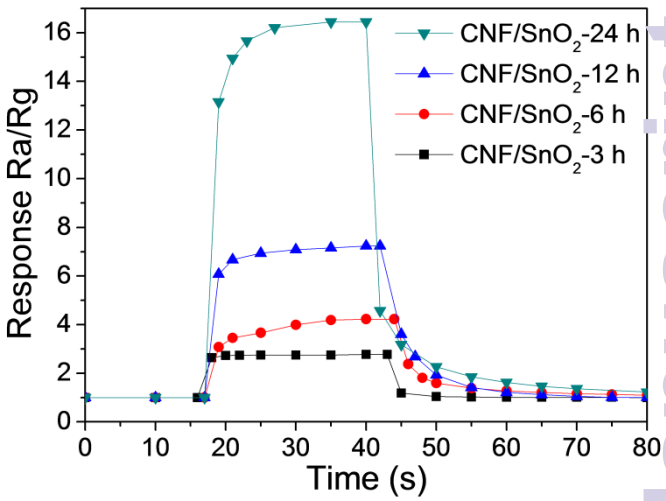

Fig. 6 Response and recovery behavior of the hierarchical p junction nanostructures with different hydrothermal reaction tir at 100 ppm H_2.

gradually as the reaction proceeded, confirming that the SnO_2 contents within the samples are 11, 19, 25 and 33 wt% corresponding to reaction time of 3, 6, 12 and 24 h, respectively.

In order to examine gas sensing properties of the prepared heterostructured nanomaterials and the effect of SnO_2 nanosheets decorated on the surface, we fabricated gas sensors and measured their resistance response. The optimum working temperature is an important functional characteristic for gas sensors. Fig. 3 presents the response of the sensors to 100 ppm of H_2 at different operating temperatures. It is clearly showing that the CNFs based sensor exhibits inert response to hydrogen gases. In our previous work, it is recognized that SnO_2-based sensors usually work at high temperature (even greater than 300 ℃) due to their high resistance.[25-26] As for the sensors of SnO_2/CNFs nanocomposite, with increasing sensing temperature, the magnitude of H_2 gas response increases and attains the maximum value at 200℃, which indirectly verifies the promotion effect of CNFs. Generally, chemical sensors have two functions: a receptor function which recognizes a chemical substance and a transducer function which transduces the chemical signal into an output signal.[27] For the present SnO_2/CNFs network sensors, it is believed that SnO_2 nanosheets identify H_2 gas (receptor function) and CNFs provide conducting path (transducer function), and then this cooperative combination allows H_2 detection at lower temperature.

Fig. 4 plots the response changes with different hydrothermal reaction times, against different concentrations of H_2 (5 ppm–3.5%). The largest response is the sample obtained with the reaction time of 24 h. The response of our samples increases rapidly with increasing H_2 concentration at first (below 15 000 ppm). After the H_2 concentration is greater than 15 000 ppm, the response begins to level off, indicating that the sensor becomes more or less saturated. Saturation concentration is different for the samples obtained from different reaction time, indicating that the saturation concentration is related to the surface area of SnO_2. Moreover, the inset in Fig. 4 shows the linear curve in the range of 1–500 ppm, which confirms that the sensor is suitable for low concentration alcohol gas detection. As selectivity is also very important for a gas sensor, Fig. 5 shows the selectivity of the optimized sensor exposed to different target gases (H_2, C_2H_5OH, CH_3COCH_3, CH_4, butane, toluene and CO) at 100 ppm. It can be clearly seen that our sensor has good selectivity to H_2 while the responses to other gases of the same concentration are significantly smaller.

The amounts and sizes of SnO_2 nanosheets on the CNF surfaces affect the sensing performance of H_2 sensor. The real-time responses of the sensors were measured by exposing to 100 ppm H_2 in which excellent sensitivities and rapid response-recovery behavior were observed (Fig. 6). These gas sensors display reversible and reproducible real-time responses. Response time is approximately 4 s for all gas sensors in 100 ppm hydrogen, and recovery time is less than 16 s. Response and recovery time a respectively defined as the time required for the sensor signal to reach 90% of the saturation and original values. Slightly changes in response and recovery time can be found with different depositing time of SnO_2 nanosheets on the CNF surface, indicating that the transformation of electric signals mainly depends on conduction of the inside CNF. However, the increase of the amounts and the sizes of SnO_2 nanosheets can improve the sensitivities and recovery time of the hybrid CNFs sensors.

Compared with the results reported in the literature, which mainly focus on the core-shell materials and simple 1D nanostructure based gas sensors, the following mechanism for the enhanced sensing performances can be established. In heterostructures, CNF plays an important role in reducing the resistance of the sensing materials, while SnO_2 nanosheet mainly controls the sensing properties.[28] Compared with the sensing performance of pure CNFs, an appropriate proportion of SnO_2 the heterostructures is necessary to obtain high gas sensitivity. On the other hand, thin SnO_2 nanosheets standing on the surface rather than gathering into microspheres (Fig. S3†) provides mo reactive points available, which is crucial to control the sensi properties (compared to the results in Fig. S4†). The oxygen adsor on the exposed surface of the SnO_2 conduction band and ionizes O^- or O^{2-}, forming depletion layers. When the sensor is exposed to

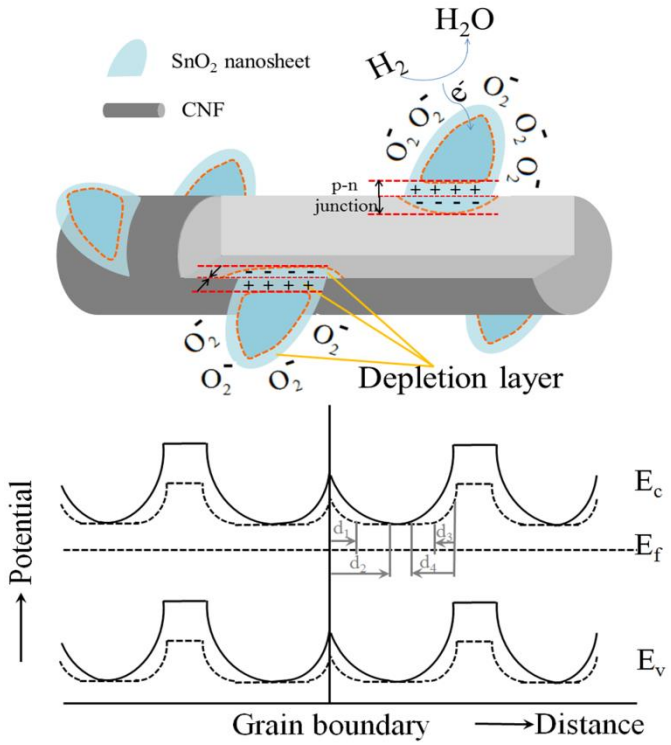

Scheme 1 Schematic illustration of potential barriers to electronic conduction at grain boundaries and at p–n heterojunctions for CNFs/SnO_2; d_1 and d_3 are depletion layer widths when exposed to hydrogen; d_2 and d_4 are depletion layer widths in air.

reducing gas such as H_2, gas molecules react with the adsorbed oxygen and release the trapped electrons back to the conduction band, causing the resistance changes.

Another track of thought to understand the enhanced mechanism based on these hybrid materials can be explained by taking into account the electrical modifications induced by the heterojunction formed at the interface between the n-SnO_2 nanosheet and the p-CNFs support. Scheme 1 depicts the changes of the electronic energy bands for CNF/SnO_2 hybrid material before and after the adsorption of H_2 gases. Two depletion layers exist: one is on the surface of the SnO_2 nanosheet, and the other is located in the interface between CNF and SnO_2. Before the H_2 gas is adsorbed, wider and higher potential barriers of these two depletion layers are given in solid line. After exposed to H_2, the barriers are changed as illustrated in the dashed line, respectively. The change in both the depletion layers at the oxide grain boundaries and the p-n heterojunction contributed to the improved sensitivity of the sensing materials. The formation of p-n heterojunction, in other words, works like an n-p-n amplifier, in which p-type CNF blocks electrons transfer from n (emitter) to n (collector), and thus decreases the barrier a little bit so as to allow a large amount of electrons to pass from emitter to collector.[29-32]

The grain size of sensing materials is an important issue. Small grain size and large specific surface area afford a greater adsorption and higher sensitivity.[33-34] According to the previous report, the depletion layer λ of the SnO_2 is estimated to be 3 nm.[35] When the dimension of SnO_2 is less than 2λ (critical size value 6 nm), the size is likely to produce a complete depletion of carriers inside.[36, 37] In the hybridized SnO_2/CNF nanostructures, SnO_2 nanosheets standing on CNFs grow larger in plane dimension, and slight change in thickness within a similar size of 6 nm. The hybrid platform as a sensing system is potentially superior to the respective component. It provides an opportunity to engineer sensing devices with quantum-mechanical attributes due to electrons transfer between the nanosheets and CNFs, which can be extended to a wide range of innovative applications as well. This new sensing scheme will be instrumental for the development of new sensors based on hybrid nanostructures.

Conclusions

In summary, we have developed a hydrothermal method to directly grow SnO_2 nanosheets on carbon nanofibers for gas sensors. The gas sensing properties of the composites were found to be dependent on the loading amount and the size of SnO_2 nanosheets. The sensor based on CNFs that experienced a hydrothermal reaction for 24 h showed the highest sensitivity. An enhanced mechanism for the synergic effect of CNFs and SnO_2 nanosheets including a p–n junction theory was established. Moreover, the heterostructure of thin SnO_2 nanosheets vertically standing on the surface of CNFs facilitate the gas sensing adequately. We believe that the present work can construct a powerful platform to better understand the relationship between the microstructures and their gas sensing performances.

Acknowledgements

The authors gratefully acknowledge the financial support by National Natural Science Foundation of China (Grant No. 51402362 and 21471160), Shandong Natural Science Foundation (ZR2014EMQ012), Qingdao Science and Technology Program for Youth (14-2-4-34-jch) and the Fundamental Research Funds for the Central Universities (14CX02161A).

Notes and references

1 N. Miura, M. Nakatou and S. Zhuiykov, *Sens. Actuators, B*, 2003, **93**, 221–228.
2 L. Liao, H. X. Mai, Q. Yuan, H. B. Lu, J. C. Li, C. Liu, C. H. Yan, Z. X. Shen and T. Yu, *J. Phys. Chem. C*, 2008, **112**, 9061–9065.
3 J. S. Lee, O. S. Kwon, S. J., E. Y. Park, S. A. You, H. Yoon, and J Jang, *ACS Nano*, 2011, **5**, 7992–8001
4 J. Yi, J. M. Lee and W. I. Park, *Sens. Actuators, B*, 2011, **155**, 264–269.
5 A. Khanna, R. Kumar and S. S. Bhatti, *Appl. Phys. Lett.*, 200[illegible], **82**, 4388–4390.
6 H. Jiang, *Small*, 2011, **7**, 2413-2427.
7 K. Pan, Y. Dong, W. Zhou, Q. Pan, Y. Xie, T. Xie, G. Tian and [illegible] Wang, *ACS Appl. Mater. Interfaces*, 2013, **5**, 8314-8320.
8 J. Shi, Y. Hara, C. Sun, M. A. Anderson and X. Wang, *Nano Lett.*, 2011, **11**, 3413-3419.

9 Z. Wang, Z. Li, X. Xu, T. Jiang, H. Zhang, W. Wang and C. Wang, *J. Mater. Chem. C*, 2013, **1**, 213-215.
10 J. W. Grebinski, K. L. Hull, J. Zhang, T. H. Kosel and M. Kuno, *Chem. Mater.*, 2004, **16**, 5260-5272.
11 W. T. Yao, S. H. Yu, S. J. Liu, J. P. Chen, X. M. Liu and F. Q. Li, *J. Phys. Chem. B*, 2006, **110**, 11704-11710.
12 D. I. Suh, S. Y. Lee, T. H. Kim, J. M. Chun, E. K. Suh, O. B. Yang and S. K. Lee, *Chem. phys. Lett.*, 2007, **442**, 348-353.
13 H. M. Cheng, W.H. Chiu, C. H. Lee, S. Y. Tsai and W. F. Hsieh, *J. Phys. Chem. C*, 2008, **112**, 16359-16364.
14 S. S. Kim, S. W. Choi, H. G. Na, D. S. Kwak, Y. J. Kwon and H. W. Kim, *Curr. Appl. Phys.*, 2013, **13**, 526-532.
15 Z. Li, H. Zhang, W. Zheng, W. Wang, H. Huang, C. Wang, A. G. MacDiarmid and Y. Wei, J. Am. Chem. Soc., 2008, **130**, 5036-5037.
16 Z. Wang, Z. Li, J. Sun, H. Zhang, W. Wang, W. Zheng and C. Wang, *J. Phys. Chem. C*, 2010, **114**, 6100-6105.
17 G. Wang, Y. Ji, X. Huang, X. Yang, P. I. Gouma and M. Dudley, *J. Phys. Chem. B*, 2006, **110**, 23777-23782.
18 J. Li, C. Papadopoulos and J. Xu, *Nature*, 1999, **402**, 253-254.
19 K. Pan, Y. Dong, W. Zhou, Q. Pan, Y. Xie, T. Xie, G. Tian and G. Wang, *ACS Appl. Mater. Interfaces*, 2013, **5**, 8314-8320.
20 J. Shi, Y. Hara, C. Sun, M. A. Anderson and X. Wang, *Nano Lett.*, 2011, **11**, 3413-3419.
21 S. W. Choi, A. Katoch, G. J. Sun and S. S. Kim, *Sensors Actuat. B-Chem.*, 2013, **181**, 787-794.
22 C. Kim, K. S. Yang, M. Kojima, K. Yoshida, Y. J. Kim, Y. A. Kim and M. Endo, *Adv. Funct. Mater.*, 2006, **16**, 2393-2397.
23 J. Li, S. Tang, L. Lu and H. C. Zeng, *J. Am. Chem. Soc.*, 2007, **129**, 9401-9409.
24 Z. Wang, Z. Li, T. Jiang, X. Xu and C. Wang, *ACS Appl. Mater. Interfaces*, 2013, **5**, 2013-2021.
25 M. M. Arafat, B. Dinan, S. A. Akbar and A. Haseeb, *Sensors*, 2012, **12**, 7207-7258.
26 Z. Chen, D. Pan, Z. Li, Z. Jiao, M. Wu, C. H. Shek, C. M. L. Wu and J. K. L. Lai, *Chem. Rev.*, 2014, **114**, 7442-7486.
27 M. Yang, D. H. Kim, W. S. Kim, T. J. Kang, B. Y. Lee, S. Hong, Y. H. Kim and S. H. Hong, *Nanotechnology*, 2010, **21**, 215501.
28 Y. Chen, C. Zhu and T. Wang, *Nanotechnology*, 2006, **17**, 3012.
29 N. Pinna, C. Marichy, M. G. Willinger, N. Donato, M. Latino and G. Neri, in Sensors and Microsystems, Springer, 2012, DOI: 10.1007/978-1-4614-0935-9_18, pp. 105-108.
30 B. Y. Wei, M. C. Hsu, P. G. Su, H. M. Lin, R. J. Wu and H. J. Lai, *Sensors Actuat. B-Chem.*, 2004, **101**, 81-89.
31 N. Van Duy, N. Van Hieu, P. T. Huy, N. D. Chien, M. Thamilselvan and J. Yi, *Physica E: Low-dimensional Systems and Nanostructures*, 2008, **41**, 258-263.
32 G. Lu, L. E. Ocola and J. Chen, *Adv. Mater.*, 2009, **21**, 2487-2491.
33 J. Xu, Q. Pan, Y. a. Shun and Z. Tian, *Sensors Actuat. B-Chem.*, 2000, **66**, 277-279.
34 K. Arshak and I. Gaidan, *Mater. Sci. Eng., B*, 2005, **118**, 44-49.
35 N. Yamazoe and N. Miura, *Chemical Sensor Technology*, 1992, **4**, 19-42.
36 E. Comini, G. Faglia, G. Sberveglieri, Z. Pan and Z. L. Wang, *Appl. Phys. Lett.*, 2002, **81**, 1869-1871.
37 Y. Wang, X. Jiang and Y. Xia, *J. Am. Chem. Soc.*, 2003, **125**, 16176-16177.